Numerical Simulation of Anomalous Penetrant Diffusion in Polymers

J. C. WU and NIKOLAOS A. PEPPAS*

School of Chemical Engineering, Purdue University, West Lafayette, Indiana 47907-1283

SYNOPSIS

This work introduces a new numerical algorithm that can be used to analyze complex problems of penetrant transport. Penetrant transport in polymers often deviates from the predictions of Fick's law because of the coupling between penetrant diffusion and the polymer mechanical behavior. This phenomenon is particularly important in glassy polymers. This leads to a model consisting of two coupled differential equations for penetrant diffusion and polymer stress relaxation, respectively. If the polymer relaxation is the rate-limiting step, both the concentration and stress profiles are very steep. A new algorithm based on a finite difference method is proposed to solve the model equations. It features the development of a tridiagonal iterative method to solve the nonlinear finite difference equations obtained from the finite difference approximation of the differential equations. This method was found to be efficient and accurate. Numerical simulation of penetrant diffusion in glassy polymers was performed, showing that the integral sorption Deborah number is a major parameter affecting the transition from Fickian to anomalous diffusion behavior.

INTRODUCTION

Diffusion of small penetrant molecules in polymeric materials is of technological importance in a variety of applications (e.g., barrier materials, controlled release, microelectronics, and environmental effect on engineering polymeric materials). Research in this field has been quite active in the last decade. It has been observed that penetrant diffusion at a temperature above the polymer's glass transition temperature usually agrees with the predictions of Fick's law. However, when the polymer is in its glassy state, penetrant diffusion often deviates from Fick's law, leading to anomalous or non-Fickian behavior. The deviation from Fickian behavior has been associated with the finite rate at which the polymer structure rearranges to accommodate penetrant molecules and has been observed for many polymer–penetrant systems.[1-3]

An important milestone in the study of anomalous diffusional behavior was the recognition by Alfrey et al.[4] of the two extremes of diffusional behavior according to the relative rates of penetrant mobility and polymer relaxation. In Case I (Fickian) diffusion, penetrant mobility is much slower than the segmental relaxation rate. In Case II diffusion, penetrant mobility is much higher than the segmental relaxation rate and the relaxation at a sharp boundary between swollen and essentially unplasticized polymer becomes the rate-determining step. Anomalous diffusion is a process with intermediate characteristics. Hopfenberg and Frisch[5] noticed that the type of diffusional behavior observed for any polymer–penetrant system varies with temperature and penetrant activity. Vrentas and collaborators[6,7] introduced the diffusional Deborah number as a means of characterizing diffusion in amorphous polymer–penetrant systems.

Many efforts have been made to develop mathematical models for Case II diffusion. For instance, the diffusion coefficient was considered a function of local concentration and stresses.[8,9] A convective term was introduced that is governed by either local penetrant concentration[10] or the local stress, which is assumed to be equal to the osmotic pressure induced by the penetrant.[11]

* To whom correspondence should be addressed.

Journal of Applied Polymer Science, Vol. 49, 1845–1856 (1993)
 CCC 0021-8995/93/101845-12

Thomas and Windle[12-14] developed a rather successful Case II diffusion model (henceforth referred to as the TW model). According to this model, the diffusional flux is proportional to both the concentration and pressure gradients. By using a simple viscous model as a constitutive equation and assuming that the local deformation is proportional to the local penetrant concentration, a third-order nonlinear partial differential equation is obtained. Because of the high nonlinearity as well as the hyperbolic nature of this equation, the finite difference method developed by Thomas and Windle[14] has been shown to be unstable.[15] Hui and Wu[16] obtained an analytical solution of the TW model by assuming that the swelling interface between the rubbery region and the glassy region has a constant velocity and the diffusion resistance in the rubbery region is negligible. Durning[17] modified the TW model by using the Maxwell model as a stress–strain constitutive equation and investigated the differential penetrant sorption in a glassy polymer. In this case, the difference between the initial penetrant concentration and the final concentration is very small so that all the model parameters can be assumed to be constant. The resultant model consists of two linear differential equations; thus, a numerical solution has been obtained. Recently, a penetrant diffusion model was developed from linear irreversible thermodynamics theory and continuum mechanics.[18] This model extends the TW model by providing a vigorous derivation of the coupling between the polymer mechanical behavior and penetrant diffusion. Integral sorption has been studied where the difference between the initial concentration and the final concentration is large and the resultant model equations are two highly nonlinear differential equations.

In the present work, a new algorithm based on a finite difference method was developed for solving the model equations for penetrant diffusion in glassy polymers. Numerical simulation of the penetrant diffusion was conducted.

MODEL DEVELOPMENT

A brief description of the penetrant transport model equations for one-dimensional diffusion and deformation is presented from the more detailed work presented elsewhere.[18]

The penetrant mass balance equations can be expressed in terms of penetrant volume fraction if ideal mixing is assumed. For one-dimensional diffusion, we have

$$\frac{\partial \nu_1}{\partial t} + \frac{\partial (\nu_1 v_{1,x})}{\partial x} = 0 \tag{1}$$

where ν_1 is the penetrant volume fraction, and $v_{1,x}$, the x component of penetrant velocity.

The penetrant chemical potential in a swollen polymer is a function of both penetrant volume fraction and osmotically induced pressure or swelling pressure. As a result, the penetrant volume diffusional flux can be obtained from linear irreversible thermodynamics. By applying the ideal mixing assumption, the volume flux with respect to the stationary coordinates is

$$\nu_1 v_{1,x} = -\left[D_{12} \frac{\partial \nu_1}{\partial x} + \frac{D_{12} \bar{V}_1 \nu_1}{RT(1-\nu_1)(1-2\chi\nu_1)} \frac{\partial P}{\partial x} \right] \tag{2}$$

where P is the swelling pressure, and x the Flory interaction parameter. This equation shows that the volume flux is proportional to both the concentration gradient and the osmotically induced pressure gradient.

The swelling pressure in the diffusional flux expression depends upon the viscoelastic property of the polymer. The relation between the swelling pressure and stresses within the polymer can be derived from the momentum balance equations. The momentum balance equations for penetrant and polymer are[19]

$$\rho_1 \frac{D_1 v_1}{Dt} = -\nabla P_1 + \rho_1 \mathbf{b}_1 + \rho_1 \mathbf{p}_1^+ \tag{3}$$

$$\rho_2 \frac{D_2 v_2}{Dt} = -\nabla P_2 + \nabla \cdot \sigma + \rho_2 \mathbf{b}_2 + \rho_2 \mathbf{p}_2^+ \tag{4}$$

In the above equations, P_i is the partial pressure of component i; σ, the stress tensor of polymer component; $\mathbf{b}_i$, the body force; and $\mathbf{p}_i^+$ is the exchange of linear momentum between components. According to momentum conservation,

$$\rho_1 \mathbf{p}_1^+ + \rho_2 \mathbf{p}_2^+ = 0 \tag{5}$$

Adding the two momentum balance equations for one-dimensional transport and neglecting the inertial and body force terms yields

$$\frac{\partial \mathbf{P}}{\partial \mathbf{x}} = \frac{\partial \sigma_{xx}}{\partial x} \tag{6}$$

The stress–strain constitutive equation used here is the Maxwell model:

$$\frac{1}{E} \frac{\partial \sigma_{xx}}{\partial t} + \frac{\sigma_{xx}}{\eta} = \frac{\partial \epsilon_{xx}}{\partial t} \tag{7}$$

where

$$\eta = \eta_0 \exp(-a_\eta \nu_1) \tag{8}$$

During penetrant diffusion, the polymer swells. The deformation gradient tensor, F_{ij}, is used to relate the deformed state to the undeformed state. This can be expressed[20] as

$$F_{ij} = \frac{\partial x_i}{\partial X_j} \tag{9}$$

where X_i (or X, Y, and Z) and x_i (or x, y, and z) are the undeformed and deformed coordinates, respectively. For one-dimensional deformation, the deformation gradient is related to the change of volume by

$$F_{11} = |\mathbf{F}| = \frac{dV}{dV_0} = \frac{1}{\nu_2} \tag{10}$$

The local strain is related to the deformation gradient by

$$\epsilon_{xx} = F_{11} - 1 = \frac{1}{\nu_2} - 1 \tag{11}$$

By substituting eqs. (2) and (6) into eq. (1), the penetrant diffusion equation is obtained:

$$\frac{\partial \nu_1}{\partial t} = \frac{\partial}{\partial x}\left[D_{12}\frac{\partial \nu_1}{\partial x}\right] + \frac{\partial}{\partial x}\left[\frac{D_{12}\bar{V}_1\nu_1}{RT(1-\nu_1)(1-2\chi\nu_1)}\frac{\partial \sigma_{xx}}{\partial x}\right] \tag{12}$$

where

$$D_{12} = D_0 \exp(a_d \nu_1) \tag{13}$$

Equation (12) is based on deformed coordinates, resulting in a moving boundary problem. It can be converted into a fixed boundary problem by expressing the model equations in terms of undeformed coordinates.[20]

Let us consider a function f, which can be the penetrant volume fraction in the present model. At any time t, f is a function of the deformed coordinate and time. The deformed coordinate is, in turn, a function of the undeformed coordinate and time. Thus,

$$f = f[x(X, t), t] \tag{14}$$

By using the chain rule, the derivative of f with respect to the undeformed coordinate is

$$\left(\frac{\partial f}{dX}\right)_t = \left(\frac{\partial f}{dx}\right)_t \left(\frac{\partial x}{dX}\right)_t \tag{15}$$

From eqs. (9) and (15), we obtain

$$\left(\frac{\partial f}{dx}\right)_t = \frac{1}{F_{11}}\left(\frac{\partial f}{dX}\right)_t = (1-\nu_1)\left(\frac{\partial f}{dX}\right)_t \tag{16}$$

Applying the above relation to eq. (12) yields

$$\frac{\partial \nu_1}{\partial t} = (1-\nu_1)\frac{\partial}{\partial X}\left[D_{12}(1-\nu_1)\frac{\partial \nu_1}{\partial X}\right] + (1-\nu_1)\frac{\partial}{\partial X}\left[\frac{D_{12}\bar{V}_1\nu_1}{RT(1-2\chi\nu_1)}\frac{\partial \sigma_{xx}}{\partial X}\right] \tag{17}$$

The polymer relaxation equation can be expressed in terms of the penetrant volume fraction by substituting eqs. (8) and (11) into eq. (7):

$$\frac{1}{E}\frac{\partial \sigma_{xx}}{\partial t} + \frac{\sigma_{xx}}{\eta \exp(-a_\eta \nu_1)} = \frac{1}{(1-\nu_1)^2}\frac{\partial \nu_1}{\partial t} \tag{18}$$

Consequently, we have two differential equations and two variables, ν_1 and σ_{xx}. The initial and boundary conditions of eqs. (17) and (18) are

$$\nu_1(t = 0, X) = 0 \tag{19}$$

$$\sigma_{xx}(t = 0, X) = 0 \tag{20}$$

$$\nu_1(t, X = L_0) = \nu_{1,eq} \tag{21}$$

$$\sigma_{xx}(t, X = L_0) = 0 \tag{22}$$

$$\frac{\partial \nu_1(t, X = 0)}{\partial X} = 0 \tag{23}$$

and

$$\frac{\partial \sigma_{xx}(t, X = 0)}{\partial X} = 0 \tag{24}$$

In eq. (21), $\nu_{1,eq}$ is the penetrant volume fraction at the polymer–penetrant interface, which is assumed to be in equilibrium with the environment. According to the Flory–Huggins theory,[21] $\nu_{1,eq}$ can be obtained by equating the chemical potential of the penetrant in the environment to that in the mixture leading to

$$\ln a_{1,0} = [\ln \nu_{1,eq} + (1-\nu_{1,eq}) + \chi(1-\nu_{1,eq})^2] \tag{25}$$

where $a_{1,0}$ is the penetrant activity in the environment.

DIMENSIONLESS FORM OF THE MODEL EQUATIONS

For easy solution and comparison purposes, these model equations are written in dimensionless form, using the characteristic diffusion time and characteristic relaxation times that are defined as

$$\tau_{\text{dif},\nu_{1,\text{eq}}} = \frac{L_0^2}{D_0 \exp(a_d \nu_{1,\text{eq}})} \tag{26}$$

$$\tau_{\text{relax},0} = \frac{\eta_0}{E} \tag{27}$$

Here, $\tau_{\text{relax},0}$ is the characteristic relaxation time in the glassy region without penetrant and $\tau_{\text{dif},\nu_{1,\text{eq}}}$ is the characteristic diffusion time in the region where the polymer is at the equilibrium swelling condition. The integral sorption Deborah number is defined as

$$De = \frac{\tau_{\text{relax},0}}{\tau_{\text{dif},\nu_{1,\text{eq}}}} = \frac{D_0 \exp(a_d \nu_{1,\text{eq}})\,\eta_0}{E L_0^2} \tag{28}$$

Note that the integral sorption Deborah number indicates the ratio of the diffusion rate in the rubbery region to the relaxation rate in the glassy region. The dimensionless length and time are defined as

$$\bar{X} = \frac{X}{L_0} \tag{29}$$

$$\theta = \frac{t}{\tau_{\text{dif},\nu_{1,\text{eq}}}} \tag{30}$$

Also, the dimensionless stress and Young's modulus are defined as

$$\bar{\sigma} = \frac{\bar{V}_1 \sigma_{xx}}{RT} \tag{31}$$

$$\bar{E} = \frac{\bar{V}_1 E}{RT} \tag{32}$$

Consequently, eq. (17) can be rewritten as

$$\frac{\partial \nu_1}{\partial \theta} = (1-\nu_1)\frac{\partial}{\partial \bar{X}}\left[f(\nu_1)\frac{\partial \nu_1}{\partial \bar{X}}\right] + (1-\nu_1)\frac{\partial}{\partial \bar{X}}\left[g(\nu_1)\frac{\partial \bar{\sigma}}{\partial \bar{X}}\right] \tag{33}$$

where

$$f(\nu_1) = (1-\nu_1)\exp[a_d(\nu_1 - \nu_{1,\text{eq}})] \tag{34}$$

and

$$g(\nu_1) = \nu_1 \exp[a_d(\nu_1 - \nu_{1,\text{eq}})]/(1 - 2\chi\nu_1) \tag{35}$$

The dimensionless form of eq. (18) is

$$\frac{1}{E}\frac{\partial \bar{\sigma}}{\partial \theta} + \frac{\bar{\sigma}}{De\bar{E}\exp(-a_\eta \nu_1)} = \frac{1}{(1-\nu_1)^2}\frac{\partial \nu_1}{\partial \theta} \tag{36}$$

The initial and boundary conditions are

$$\nu_1(\theta = 0, \bar{X}) = 0 \tag{37}$$

$$\bar{\sigma}(\theta = 0, \bar{X}) = 0 \tag{38}$$

$$\nu_1(\theta, \bar{X} = 1) = \nu_{1,\text{eq}} \tag{39}$$

$$\bar{\sigma}(\theta, \bar{X} = 1) = 0 \tag{40}$$

$$\frac{\partial \nu_1(\theta, \bar{X} = 0)}{\partial \bar{X}} = 0 \tag{41}$$

$$\frac{\partial \bar{\sigma}(\theta, \bar{X} = 0)}{\partial \bar{X}} = 0 \tag{42}$$

NUMERICAL SOLUTION

The model equations consist of one nonlinear partial differential equation (PDE) and one nonlinear ordinary differential equation (ODE). The two equations are coupled. Both finite difference methods and finite element methods can be used to solve the above equations.

Finite difference methods use finite difference expression to approximate the derivatives in the differential equations, giving rise to simple numerical formulation. However, there are two major difficulties in applying the methods. The first difficulty is that the finite difference methods may suffer[22] from the numerical oscillation or numerical diffusion (dispersion). This becomes a serious problem in solving diffusive-convective PDEs, where the convective term predominates and a moving front travels at a constant velocity. The second problem arises from nonlinear PDEs that generate a set of nonlinear finite difference equations at each time step. The common methods for solving these nonlinear finite difference equations are the quasi-linearization, Newton, and predictor-corrector methods. The above methods become very inefficient for systems

with stiff concentration profiles. This is because a large number of grid points is required so that a large set of nonlinear finite difference equations is required to be solved.

To deal with the above problems, finite element methods have been used. The major advantage of these methods is that fewer grid points are required because high-order polynomials can be used. In addition, moving elements can also be used to follow a moving front to further reduce the grid points. However, the numerical formulation and computer programming are generally quite complicated.

The two major difficulties associated with finite difference methods can also be overcome by improving conventional finite difference methods. Recently, it has been shown that the numerical oscillation and numerical dispersion can be significantly reduced if the three-point backward finite differences scheme is used to approximate the convective term in a convective-predominant PDE.[23] It has also been demonstrated that for a set of diffusive-convective PDEs with nonlinear reaction terms a two-step expansion technique can be used to linearize the nonlinear finite difference equations so that the coefficient matrix of the resultant equations can be arranged into a tridiagonal form. A special Gauss elimination method, called the tridiagonal matrix method, can be used to solve these equations with minimum computer time and storage space.[24] As a result, the finite difference method is highly efficient.

The same methodology is to be applied in the present work to solve eqs. (33)-(42). It is instructive to notice that there are two major differences between eq. (33) and a diffusive-convective PDE with a nonlinear reaction term. The first is the second-order nature of the stress term in eq. (33) that causes less numerical oscillation or numerical dispersion than that of the first-order convective term. Thus, the conventional second-order finite difference scheme can be directly applied. The second difference is that the nonlinearity in eqs. (33) and (36) is due to the concentration dependence of diffusion coefficient and viscosity, instead of a nonlinear reaction term. As a result, an efficient solution technique, instead of the two-step expansion technique, needs to be developed to solve a set of nonlinear finite difference equations. To deal with this problem, a tridiagonal iterative method is developed in this section.

The development of the numerical method is divided into two parts: In the first part, a finite difference method is developed for solving eqs. (33)-(42) with the Young's modulus, E, being infinite. In this case, the Maxwell model described by eq. (18) is reduced to the viscous model (the same as that used in the TW model).

$$\frac{\sigma_{xx}}{\eta \exp(-\alpha_\eta \nu_1)} = \frac{1}{(1-\nu_1)^2}\frac{\partial \nu_1}{\partial t} \tag{43}$$

The dimensionless form of the above is

$$\bar{\sigma} = \frac{B \exp(-a_\eta \nu_1)}{(1-\nu_1)^2}\frac{\partial \nu_1}{\partial \theta} \tag{44}$$

Here, B is defined as

$$B = \frac{D_0 \exp(a_d \nu_{1,eq}) \eta_0 \bar{V}_1}{RTL_0^2} \tag{45}$$

By substituting eq. (44) into eq. (33), only one partial differential equation need be solved:

$$\frac{\partial \nu_1}{\partial \theta} = (1-\nu_1)\frac{\partial}{\partial \bar{X}}\left[f(\nu_1)\frac{\partial \nu_1}{\partial \bar{X}}\right] + (1-\nu_1)\frac{\partial}{\partial \bar{X}}\left\{g(\nu_1)\frac{\partial}{\partial \bar{X}}\left[h(\nu_1)\frac{\partial \nu_1}{\partial \theta}\right]\right\} \tag{46}$$

Here, $f(\nu_1)$ and $g(\nu_1)$ are the same as defined in eqs. (34) and (35). The function $h(\nu_1)$ is defined as

$$h(\nu_1) = \frac{B \exp(-a_\eta \nu_1)}{(1-\nu_1)^2} \tag{47}$$

This equation is very similar to that derived in the TW model.[16] The initial and boundary conditions for eq. (46) are

$$\nu_1(\theta = 0, \bar{X}) = 0 \tag{48}$$

$$\nu_1(\theta, \bar{X} = 1) = \nu_{1,eq} \tag{49}$$

$$\frac{\partial \nu_1(\theta, \bar{X} = 0)}{\partial \bar{X}} = 0 \tag{50}$$

The accuracy and stability of the numerical method is then tested by solving a similar partial differential equation with a known analytical solution.

In the second part, the numerical method developed in the first part will be extended to solve eqs. (33)-(42).

Part 1: Finite Difference Scheme for Solving Eqs. (46)-(50)

The finite difference approximation of the first derivative on the right side of equation (46) gives

$$\frac{\partial}{\partial \bar{X}}\left[f(v_1)\frac{\partial v_1}{\partial \bar{X}}\right] = \frac{f_j^{n+1}\Delta v_j^{n+1} - f_{j-1}^{n+1}\Delta v_{j-1}^{n+1}}{\Delta \bar{X}^2} \quad (51)$$

where v_j^n is the volume fraction of solvent at grid point j and time step n; subscript 1 is neglected. The finite difference approximation of the second derivative is

$$\frac{\partial}{\partial \bar{X}}\left\{g(v_1)\frac{\partial}{\partial \bar{X}}\left[h(v_1)\frac{\partial v_1}{\partial \theta}\right]\right\} = \frac{g_j^{n+1}\Delta H_j^{n+1} - g_{j-1}^{n+1}\Delta H_{j-1}^{n+1}}{\Delta \bar{X}^2} \quad (52)$$

Consequently, the implicit finite difference scheme of eq. (46) can be written as

$$v_j^{n+1} - v_j^n = r_1(f_j^{n+1}\Delta v_j^{n+1} - f_{j-1}^{n+1}\Delta v_{j-1}^{n+1}) + r_1(g_j^{n+1}\Delta H_j^{n+1} - g_{j-1}^{n+1}\Delta H_{j-1}^{n+1}) \quad (53)$$

where

$$r_1 = \frac{\Delta\theta(1 - v_1)}{(\Delta \bar{X})^2} \quad (54)$$

$$\Delta v_j^{n+1} = v_{j+1}^{n+1} - v_j^{n+1} \quad (55)$$

$$\Delta H_j^{n+1} = H_{j+i}^{n+1} - H_j^{n+1} \quad (56)$$

$$H_j^{n+1} = h_j^{n+1}\left(\frac{\partial v}{\partial \theta}\right)_j^{n+1} = h_j^{n+1}\frac{v_j^{n+1} - v_j^n}{\Delta\theta} \quad (57)$$

Substituting the above equations into eq. (53) and defining r_2 as

$$r_2 = \frac{(1 - v_1)}{(\Delta \bar{X})^2} \quad (58)$$

we have

$$\begin{aligned} v_j^{n+1} - v_j^n = {} & r_1[f_j^{n+1}(v_{j+1}^{n+1} - v_j^{n+1}) \\ & - f_{j-1}^{n+1}(v_j^{n+1} - v_{j-1}^{n+1})] + r_2\{g_j^{n+1}[h_{j+1}^{n+1}(v_{j+1}^{n+1} - v_{j+1}^n) \\ & - h_j^{n+1}(v_j^{n+1} - v_j^n)]\} - r_2\{g_{j-1}^{n+1}[h_j^{n+1}(v_j^{n+1} - v_j^n) \\ & - h_{j-1}^{n+1}(v_{j-1}^{n+1} - v_{j-1}^n)]\} \end{aligned} \quad (59)$$

The above equation is highly nonlinear. It is very difficult to obtain a stable solution with the commonly used predictor–corrector iterative methods. To cope with this problem, a tridiagonal iterative method is developed.

First, we rearrange eq. (59) into a tridiagonal form:

$$\begin{aligned} & (-r_1 f_{j-1}^{n+1} - r_2 g_{j-1}^{n+1} h_{j-1}^{n+1})v_{j-1}^{n+1} + (1 + r_1 f_j^{n+1} \\ & \quad + r_1 f_{j-1}^{n+1} + r_2 g_j^{n+1} h_j^{n+1} + r_2 g_{j-1}^{n+1} h_j^{n+1})v_j^{n+1} \\ & \quad + (-r_1 f_j^{n+1} - r_2 g_j^{n+1} h_{j+1}^{n+1})v_{j+1}^{n+1} \\ & = v_j^n - r_2 g_j^{n+1} h_{j+1}^n v_{j+1}^n + (r_2 g_j^{n+1} h_j^{n+1} \\ & \qquad + r_2 g_{j-1}^{n+1} h_j^{n+1})v_j^n - r_2 g_{j-1}^{n+1} h_{j-1}^{n+1} v_{j-1}^n \end{aligned} \quad (60)$$

Then, we use the following iterative method to solve the above equation:

(i) Set $(v_j^{n+1})_{k=0} = v_j^n$; k is the number of iteration.
(ii) Evaluate $(f_j^{n+1})_k$, $(g_j^{n+1})_k$, and $(h_j^{n+1})_k$ and solve eq. (60) by the tridiagonal matrix method to obtain $(v_j^{n+1})_k$ (24).
(iii) If $|(v_j^{n+1})_{k+1} - (v_j^{n+1})_k| > \epsilon$,
then
$(v_j^{n+1})_k = (v_j^{n+1})_{k+1}$,
$k = k + 1$;
goto ii);
If $|(v_j^{n+1})_{k+1} - (v_j^{n+1})_k| < \epsilon$,
then
$v_j^{n+1} = (v_j^{n+1})_{k+1}$
$v_j^n = v_j^{n+1}$;
goto i)

The accuracy and the stability of this numerical method can be tested by solving the following equation:

$$\frac{\partial v_1}{\partial \theta} = \frac{\partial}{\partial X}\left[f\frac{\partial v_1}{\partial X}\right] + \frac{\partial}{\partial X}\left\{g\frac{\partial}{\partial X}\left[h\frac{\partial v_1}{\partial \theta}\right]\right\} + r(\theta, X) \quad (61)$$

When f, g, and h are constants and $r(\theta, X)$ is equal to

$$r(\theta, X) = k\cos k(X + \theta) + k^3 gh\cos k(X + \theta) + k^2 f\sin k(X + \theta) \quad (62)$$

the analytical solution is

$$v_1(\theta, X) = \sin k(X + \theta) \quad (63)$$

The analytical solution can be compared with the numerical solution obtained with the finite differ-

ence method. The initial and boundary conditions are

$$\nu_1(0, X) = \sin kX \tag{64}$$

$$\nu_1(\theta, 0) = \sin k\theta \tag{65}$$

$$\nu_1(\theta, 2\pi) = \sin k\theta \tag{66}$$

If k is equal to 4, the results are shown in Figure 1. It is seen that the numerical solution is very close to the analytical solution. The effects of spatial and temporal step sizes on accuracy of the solution as well as on the computer time are shown in Table I. It is seen that as the number of grids increases the accuracy of the solution increases. Because the temporal derivative is approximated by a first-order difference scheme and the spatial derivatives are approximated by a second-order difference scheme, a smaller temporal step size is needed. The temporal step size can be further reduced if a higher-order difference scheme such as the three-point backward scheme is used.[23] Little CPU time is needed for all these cases. This demonstrates the high efficiency of the numerical method.

The solutions obtained from the above numerical procedure give the penetrant volume fraction based on the undeformed spatial coordinate. To describe the dynamic swelling or deformation of the polymer matrix, it is necessary to express the penetrant volume fraction based on the deformed coordinate. This can be done by integrating eq. (9):

$$x_j = \int_0^{X_j} F_{11}\, dX \tag{67}$$

After the concentration profiles are obtained, the stress profiles can be calculated from eq. (44). The fractional mass uptake is determined by the following integration:

$$\frac{M_t}{M_\infty} = \frac{\int_0^L \nu_1 F_{11}\, dX}{\nu_{1,\mathrm{eq}} F_{11} L_0} \tag{68}$$

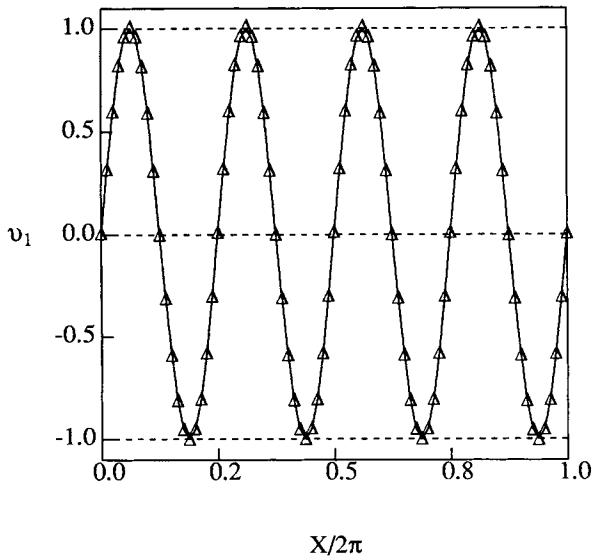

Figure 1 Comparison between the analytical and numerical solutions of eq. (61) at $\theta = \pi$. The continuous curve is the analytical solution that is $\nu_1 = \sin 4(X + \theta)$. $\Delta\theta = 2\pi/1000$; $\Delta X = 2\pi/80$.

Table I Effect of Grid Size on Accuracy and CPU Time of Numerical Solution

No. Temporal Grid Points	No. Spatial Grid Points	Average[a] Relative Error	CPU Time[b] (s)
200	32	5.43%	0.9
1000	32	4.68%	4.4
1000	80	1.54%	10.7

[a] The average relative error is calculated by $r_{\mathrm{ave}} = (1/N)\sum_1^N [(u_{i,\mathrm{ana}} - u_{i,\mathrm{cal}})/u_{i,\mathrm{ana}}]$, where the points where $u_{i,\mathrm{ana}}$ is zero are not included.

[b] Sun Sparc station 2 was used.

Part 2: Finite Difference Scheme for Solving Eqs. (33)-(42)

When the Maxwell model is used, a system of one partial differential equation and one ordinary differential equation need to be solved. Nevertheless, a similar numerical procedure can be used.

First, the implicit finite difference scheme of eq. (33) is written as

$$\nu_j^{n+1} - \nu_j^n = r_1(f_j^{n+1}\Delta\nu_j^{n+1} - f_{j-1}^{n+1}\Delta\nu_{j-1}^{n+1}) + r_1(g_j^{n+1}\Delta\bar{\sigma}_j^{n+1} - g_{j-1}^{n+1}\Delta\bar{\sigma}_{j-1}^{n-1}) \tag{69}$$

where

$$r_1 = \frac{\Delta\theta(1 - \nu_1)}{(\Delta\bar{X})^2} \tag{70}$$

$$\Delta\nu_j^{n+1} = \nu_{j+1}^{n+1} - \nu_j^{n+1} \tag{71}$$

$$\Delta\bar{\sigma}_j^{n+1} = \bar{\sigma}_{j+1}^{n+1} - \bar{\sigma}_j^{n+1} \tag{72}$$

The finite difference scheme of eq. (36) can be expressed as

$$\bar{\sigma}_j^{n+1} - \bar{\sigma}_j^n = -\frac{\bar{\sigma}_j^{n+1}\Delta\theta}{De\exp(-a_\eta \nu_j^{n+1})} + \frac{\bar{E}}{(1+\nu_j^{n+1})^2}(\nu_j^{n+1} - \nu_j^n) \quad (73)$$

Then, eq. (73) is rearranged into

$$\bar{\sigma}_j^{n+1} = q_j^{n+1}\bar{\sigma}_j^n + h_j^{n+1}(\nu_j^{n+1} - \nu_j^n) \quad (74)$$

where

$$q_j^{n+1} = \frac{De}{De + \Delta\theta\exp(a_\eta \nu_j^{n+1})} \quad (75)$$

$$h_j^{n+1} = \frac{De\bar{E}}{(1-\nu_j^{n+1})^2[De + \Delta\theta\exp(a_\eta \nu_j^{n+1})]} \quad (76)$$

Substituting eq. (74) into eq. (69) yields

$$\begin{aligned}\nu_j^{n+1} - \nu_j^n = {} & r_1[f_j^{n+1}(\nu_{j+1}^{n+1} - \nu_j^{n+1}) \\ & - f_{j-1}^{n+1}(\nu_j^{n+1} - \nu_{j-1}^{n+1})] + r_1\{g_j^{n+1}[h_{j+1}^{n+1}(\nu_{j+1}^{n+1} \\ & - \nu_{j+1}^n) - h_j^{n+1}(\nu_j^{n+1} - \nu_j^n) \\ & - r_1\{g_{j-1}^{n+1}[h_j^{n+1}(\nu_j^{n+1} - \nu_j^n) - h_{j-1}^{n+1}(\nu_{j-1}^{n+1} \\ & - \nu_{j-1}^n)]\} + r_1[g_{j+1}^{n+1}(q_{j+1}^{n+1}\bar{\sigma}_{j+1}^n - q_j^{n+1}\bar{\sigma}_j^n) \\ & - g_j^{n+1}(q_j^{n+1}\bar{\sigma}_j^n - q_{j-1}^{n+1}\bar{\sigma}_{j-1}^n)] \end{aligned} \quad (77)$$

This equation is similar to eq. (59). Thus, the tridiagonal iterative method developed before can be employed. By rearranging eq. (77) into a tridiagonal form, we have

$$\begin{aligned}& (-r_1 f_{j-1}^{n+1} - r_2 g_{j-1}^{n+1} h_{j-1}^{n+1})\nu_{j-1}^{n+1} + (1 + r_1 f_j^{n+1} \\ & \quad + r_1 f_{j-1}^{n+1} + r_2 g_j^{n+1} h_j^{n+1} + r_2 g_{j-1}^{n+1} h_j^{n+1})\nu_j^{n+1} \\ & \quad + (-r_1 f_j^{n+1} - r_2 g_j^{n+1} h_{j+1}^{n+1})\nu_{j+1}^{n+1} \\ & = \nu_j^n - r_2 g_j^{n+1} h_{j+1}^n \nu_{j+1}^n + (r_2 g_j^{n+1} h_j^{n+1} \\ & \quad + r_2 g_{j-1}^{n+1} h_j^{n+1})\nu_j^n - r_2 g_{j-1}^{n+1} h_{j-1}^{n+1}\nu_{j-1}^n \\ & \quad + r_1[g_{j+1}^{n+1}(q_{j+1}^{n+1}\bar{\sigma}_{j+1}^n - q_j^{n+1}\bar{\sigma}_j^n) \\ & \quad - g_{j-1}^{n+1}(q_j^{n+1}\bar{\sigma}_j^n - q_{j-1}^{n+1}\bar{\sigma}_{j-1}^n)] \end{aligned} \quad (78)$$

Then, the same iterative procedure as that used in solving eq. (60) can be applied to solve eq. (78).

RESULTS AND DISCUSSION

To show the capabilities of the new algorithm, we present here a number of numerical simulations of importance to the broad transport problem. There are six model parameters in the dimensionless model equations. A typical set of model parameters is listed in Table I. In this table, the Flory interaction parameter, χ, is assumed to be 0.9, corresponding to diffusion of good swelling agents that can substantially swell a polymer but cannot dissolve it. The resultant penetrant equilibrium volume fraction is $\nu_{1,eq} = 0.383$, which is obtained from eq. (25). The penetrant activity in the bulk penetrant phase is $a_{1,0} = 1.0$ for a pure penetrant. The exponential factor of the diffusion coefficient, a_d, is taken to be 20 so that the diffusion coefficient in the rubbery region is about three orders of magnitude larger than that in the glassy region. The exponential factor of viscosity, a_η, is taken to be 50 so that the viscosity changes from 4×10^{12} to about 1.5×10^7 N s m^{-2}. The value of De and $\bar{E}$ are calculated from eqs. (28) and (32). The parameters needed are also listed in Table II.

Simulation results using these parameters are shown in Figures 2–5, exhibiting typical Case II diffusional behavior. In figure 2, the normalized penetrant volume fraction is plotted against the normalized position. The center of the swelling slab is at $x/L_0 = 0$. The penetrant–polymer boundary is initially at $x/L_0 = 1$. It is seen that the concentration changes dramatically at the interface between the rubbery region and glassy region, indicating that the relaxation of the polymer matrix is the rate-determining step of the whole process. In the rubbery region, the concentration profiles are quite flat, showing the fast diffusion rate.

It is interesting to note that the concentration

Table II A Set of Model Parameters for Numerical Simulation

χ	0.90
$a_{1,0}$	1.0
a_d	20
a_η	50
De	4.54
$\bar{E}$	12.11
D_0	4.0×10^{-14} m^2 s^{-1}
η_0	4.0×10^{12} N s m^{-2}
E	3.0×10^8 N m^{-2}
L	5.9×10^{-4} m
T	297 K
$\bar{V}_1$	4.04×10^{-5} m^3 mol^{-1}

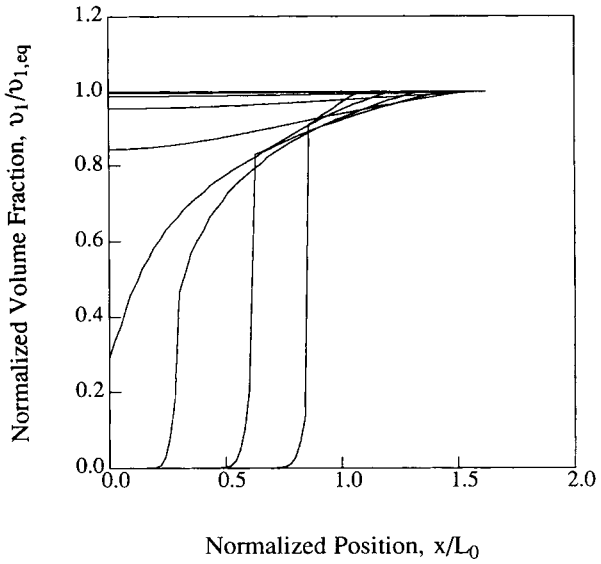

Figure 2 Normalized penetrant volume fraction as a function of normalized position. The model parameters are listed in Table II. The position of $x/L_0 = 0$ is the center of the slab and the time increment starting from the first curve on the right is $\Delta\theta = 7.2$.

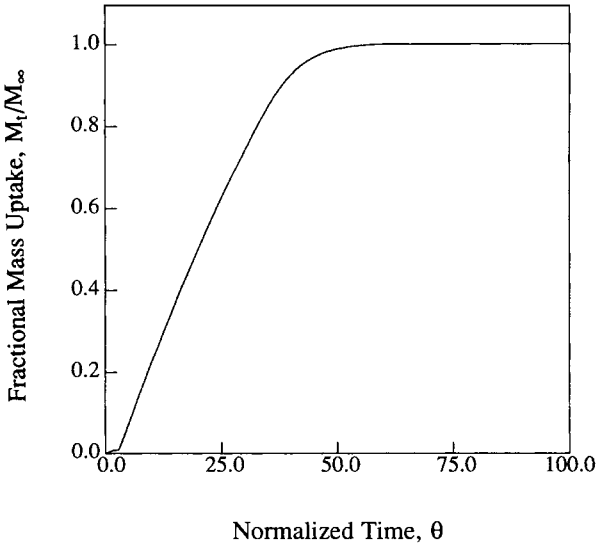

Figure 4 Internal stress as a function of normalized position. The model parameters are listed in Table II. The position of $x/L_0 = 0$ is the center of the slab and the time increment starting from the first curve on the right is $\Delta\theta = 7.2$.

profiles do not seem continuous. This is because the diffusion rate is much greater than the relaxation rate so that the glassy core behaves like an impervious wall, resulting in a concave curve. As the diffusion front moves inward and the rubbery region swells outward, the diffusion resistance increases. Consequently, the concentration profiles become smoother.

Figure 3 shows the penetrant volume fraction profiles plotted against the undeformed normalized

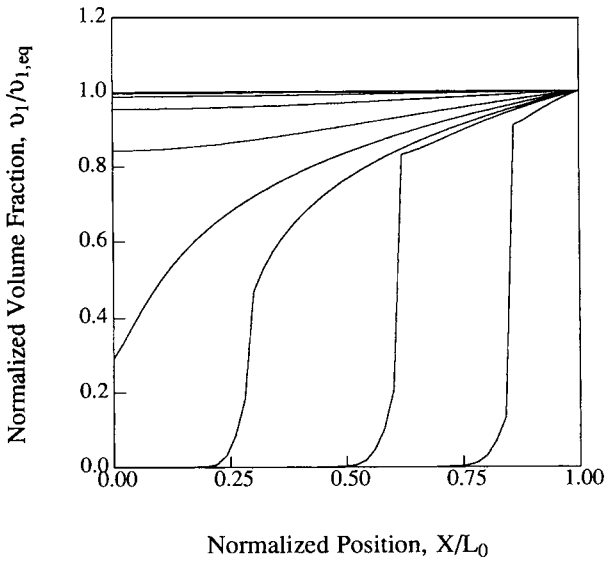

Figure 3 Normalized penetrant volume fraction as a function of the undeformed normalized position. The model parameters are listed in Table II. The position of $X/L_0 = 0$ is the center of the slab and the time increment starting from the first curve on the right is $\Delta\theta = 7.2$.

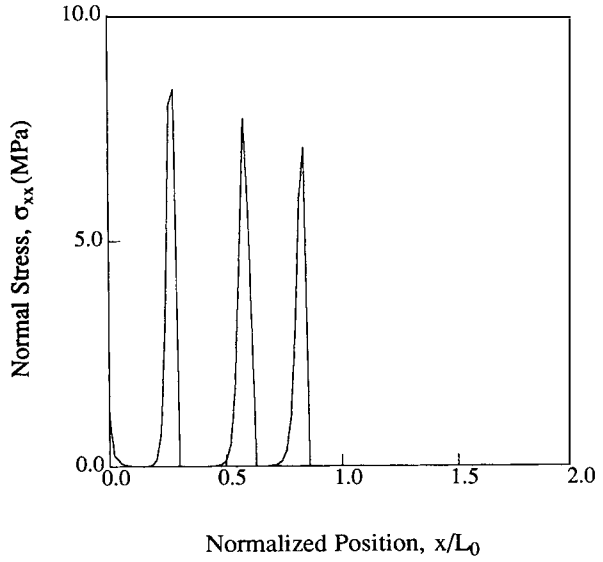

Figure 5 Fractional mass uptake as a function of normalized time. The model parameters are listed in Table II.

position. These results are the solutions of eq. (33)–(42). The profiles in Figure 2 were obtained by using eq. (67) to transform the volume fractions based on the undeformed coordinates into those based on the deformed coordinates.

The fractional mass uptake curve is plotted in Figure 4, showing a linear relation between the mass uptake and time, which is a major indication of Case II diffusion. The Deborah number in this case is about 4.54, indicating the relaxation time is much longer than the diffusion time. It is noted that an induction time exists before the interface forms and moves into the bulk of the polymer sample.

The stress profiles are shown in Figure 5. The internal stress level is about 10 MPa. This value is close to the range for crazing. It is seen that the maximum stress appears near the interface. In the swollen region, the stress is negligible.

Because of the very stiff concentration profiles, a large number of grid points is required for finite difference methods. In the above stimulation, 100 spatial grid points and 2000 temporal grids points are used. The Sun Sparc station II was used and the CPU time was 22.3 s. This demonstrates the high efficiency of the numerical method.

In eq. (28), the diffusion Deborah number is defined as a ratio of the polymer relaxation time to the penetrant diffusion time. If the relaxation time is reduced, the Deborah number will decrease. As a result, a transition from the Case II diffusion to the Fickian diffusion will be observed; this is shown in Figures 6 and 7. If all the parameters in Table II remain unchanged except that η_0 is decreased from 4.0×10^{12} to 10^{11} N s m^{-2}, the Deborah number is decreased from 4.54 to 0.11. As a result, the relaxation rate becomes very fast and the diffusion rate becomes the rate-limiting step. As shown in Figure 6, the concentration profiles become very smooth. Also, the mass uptake is proportional to square root of time at the initial sorption stage, as shown in Figure 7. These are two typical features of Fickian diffusion. Further discussion of the numerical results as well as comparison with selected data are presented elsewhere.[25]

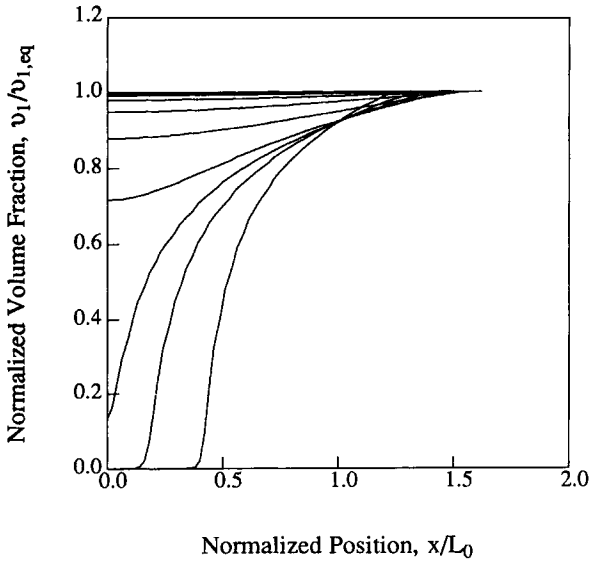

Figure 6 Normalized penetrant volume fraction as a function of normalized position. The model parameters are listed in Table II except that $\eta_0 = 10^{11}$ N s m^{-2} and $De = 0.11$. The position of $x/L_0 = 0$ is the center of the slab and the time increment from the first curve on the right is $\Delta\theta = 6.0$.

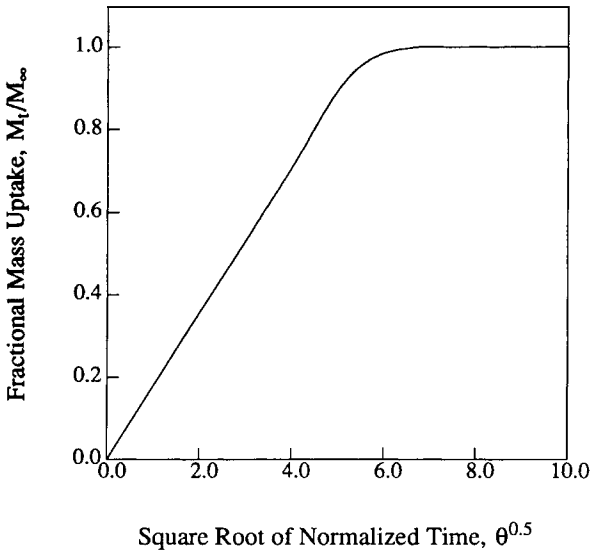

Figure 7 Fractional mass uptake as a function of the square root of normalized time. The model parameters are listed in Table II except that $\eta_0 = 10^{11}$ N s m^{-2} and $De = 0.11$.

CONCLUSIONS

An implicit finite difference method was developed to solve the model equations for one-dimensional penetrant diffusion in glassy polymers, which consist of one nonlinear partial differential equation and one nonlinear ordinary differential equation. The unique feature of this method is the development of a tridiagonal iterative method to solve the finite difference equations obtained from the finite difference

approximation of the differential equations. As a result, only a system of linear equations is solved at each iteration so that it allows a large number of grid points. In addition, good convergence is obtained when the finite difference equations are solved at each time step, giving rise to a stable solution.

Numerical simulation of penetrant diffusion in glassy polymers was performed. The simulation results show the typical Case II diffusional behavior as well as the transition from Case II to Fickian diffusion. The integral sorption Deborah number was shown to be a major parameter affecting penetrant diffusional behavior.

The authors wish to thank Professor E. N. Houstis of the Computer Science Department of Purdue University for his comments on seeking an analytical solution to testing the numerical method. This work was supported in part by a grant from the National Science Foundation.

NOTATION

a_d	exponential factor for diffusion coefficient
a_η	exponential factor for viscosity
$a_{1,0}$	penetrant activity in environment
$\mathbf{b}_i$	body force of component i
D_{12}	penetrant diffusion coefficient
D_0	penetrant diffusion coefficient at zero penetrant concentration
De	integral sorption Deborah number
E	Young's modulus
$\bar{E}$	dimensionless Young's modulus
F_{ij}	component of deformation gradient tensor
L	half-thickness of a polymer film at time t
L_0	half-thickness of a polymer film at time $t = 0$
M_t	total mass uptake at time t
M_∞	total mass uptake at equilibrium conditions
P	swelling pressure or total pressure
P_1	partial pressure of penetrant
P_2	partial pressure of polymer
$\mathbf{p}_i^+$	momentum exchange between component i and other components
t	time
T	temperature
$\mathbf{v}_i$	velocity vector of component i
V	deformed total volume
V_0	undeformed total volume
$\bar{V}_i$	molar volume of component i
x_i	component of position vector in deformed coordinates, whose components are x, y, z, or x_1, x_2, x_3
X_i	Component of position vector in undeformed coordinates, whose components are X, Y, Z, or X_1, X_2, X_3
$\bar{X}$	dimensionless length based on undeformed coordinates
ϵ_{ij}	Small strain component
η	viscosity of the dashpot in the Maxwell model
η_0	viscosity of the dashpot in the Maxwell model at zero penetrant concentration
θ	dimensionless time
ρ_i	mass of component i per unit volume
σ	stress tensor on polymer
σ_{ij}	stress components of stress tensor of polymer component
$\bar{\sigma}$	dimensionless normal stress in x direction
$\tau_{\mathrm{dif},\nu_{1,\mathrm{eq}}}$	characteristic diffusion time defined at equilibrium swelling conditions
$\tau_{\mathrm{relax},0}$	characteristic relaxation time defined zero penetrant volume fraction
ν_i	volume fraction of component i
$\nu_{1,\mathrm{eq}}$	volume fraction of component 1 at equilibrium conditions
χ	Flory polymer–penetrant interaction parameter

REFERENCES

1. F. A. Long and D. J. Richman, *J. Am. Chem. Soc.*, **82,** 513 (1960).
2. T. K. Kwei and H. M. Zupko, *J. Polym. Sci. A-2,* **7,** 867 (1969).
3. H. B. Hopfenberg, R. H. Holley, and V. Stannett, *Polym. Eng. Sci.*, **9,** 242 (1969).
4. T. Alfrey Jr., E. F. Gurnee, and W. G. Lloyd, *J. Polym. Sci. C,* **12,** 249 (1966).
5. H. B. Hopfenberg and H. L. Frisch, *J. Polym. Sci. Polym. Phys. Ed.*, **7,** 405 (1969).
6. J. S. Vrentas, C. M. Jarzebski, and J. L. Duda, *AIChE J.*, **21,** 894 (1975).
7. J. S. Vrentas and J. L. Duda, *J. Polym. Sci. Polym. Phys. Ed.*, **15,** 441 (1977).
8. J. Crank, *J. Polym. Sci.*, **11,** 151 (1953).
9. J. H. Petropoulos and P. P. Roussis, *J. Membr. Sci.*, **3,** 343 (1978).
10. G. Astarita and G. C. Sarti, *Polym. Eng. Sci.*, **18,** 388 (1978).
11. G. C. Sarti, *Polymer,* **20,** 827 (1979).
12. N. L. Thomas and A. H. Windle, *Polymer,* **21,** 613 (1980).
13. N. L. Thomas and A. H. Windle, *Polymer,* **22,** 627 (1981).
14. N. L. Thomas and A. H. Windle, *Polymer,* **23,** 529 (1982).

15. A. H. Windle, in *Polymer Permeability,* J. Comyn, Ed., Elsevier, London, 1985, p. 75.
16. C. Y. Hui and K. C. Wu, *J. Appl. Phys.,* **61,** 5137 (1987).
17. C. J. Durning, *J. Polym. Sci. Polym. Phys. Ed.,* **23,** 1831 (1985).
18. J. C. Wu and N. A. Peppas, *J. Polym. Sci. Polym. Phys. Ed.,* to appear.
19. I. Mueller, *Arch. Rat. Mech. Anal.,* **28,** 1 (1968).
20. L. E. Malvern, *Introduction to the Mechanics of a Continuous Medium,* Prentice-Hall, New Jersey, 1969.
21. P. J. Flory, *Principles of Polymer Chemistry,* Cornell University Press, Ithaca, NY, 1953.
22. B. A. Finlayson, *Nonlinear Analysis in Chemical Engineering,* McGraw-Hill, New York, 1980.
23. J. C. Wu, L. T. Fan, and L. E. Erickson, *Comput. Chem. Eng.,* **14,** 679 (1990).
24. G. D. Smith, *Numerical Solution of Partial Differential Equations: Finite Difference Methods,* Clarendon Press, Oxford, 1985.
25. J. C. Wu and N. A. Peppas, *Macromolecules,* to appear.

Received November 13, 1992
Accepted January 19, 1993